Front. Mech. Eng. 2023, 18(2): 32
https://doi.org/10.1007/s11465-023-0748-0

RESEARCH ARTICLE

Digital twin-assisted gearbox dynamic model updating toward fault diagnosis

Jingyan XIA[a], Ruyi HUANG[b,c], Yixiao LIAO[a], Jipu LI[a], Zhuyun CHEN[a,c], Weihua LI (✉)[a,b,c]

[a] *School of Mechanical and Automotive Engineering, South China University of Technology, Guangzhou 510641, China*
[b] *Shien-Ming Wu School of Intelligent Engineering, South China University of Technology, Guangzhou 511442, China*
[c] *Guangdong Artificial Intelligence and Digital Economy Laboratory (Guangzhou), Guangzhou 510335, China*

✉ *Corresponding author. E-mail: whlee@scut.edu.cn (Weihua LI)*

ABSTRACT One of the core challenges of intelligent fault diagnosis is that the diagnosis model requires numerous labeled training datasets to achieve satisfactory performance. Generating training data using a virtual model is a potential solution for addressing such a problem, and the construction of a high-fidelity virtual model is fundamental and critical for data generation. In this study, a digital twin-assisted dynamic model updating method for fault diagnosis is thus proposed to improve the fidelity and reliability of a virtual model, which can enhance the generated data quality. First, a virtual model is established to mirror the vibration response of a physical entity using a dynamic modeling method. Second, the modeling method is validated through a frequency analysis of the generated signal. Then, based on the signal similarity indicator, a physical–virtual signal interaction method is proposed to dynamically update the virtual model in which parameter sensitivity analysis, surrogate technique, and optimization algorithm are applied to increase the efficiency during the model updating. Finally, the proposed method is successfully applied to the dynamic model updating of a single-stage helical gearbox; the virtual data generated by this model can be used for gear fault diagnosis.

KEYWORDS digital twin, gearbox, model construction, model updating, physical–virtual interaction

1 Introduction

Gearboxes are widely used in industrial power-transmission applications. Different faults may naturally occur when this industrial equipment operates in harsh environments or under varying working conditions [1,2]. To guarantee operational stability and reduce maintenance costs, many fault diagnosis and condition monitoring approaches have been proposed, such as signal processing-based [3,4] and data-driven methods [5,6], which have recently attracted increased attention in academia and the industry [7,8]. Deep learning-based methods, a popular data-driven approach, have been successfully employed in different fault diagnosis tasks owing to their powerful performance in feature extraction [9,10]. However, the capability of these methods is restricted by training data quality [11–13], which may lead to poor performance in real-life engineering applications.

Benefiting from advances in simulations and computations, a promising solution can be adopted to obtain training data from virtual space. Specifically, simulation data generated by virtual models operated at any speed and load can be used to supplement the training data during the construction of a fault diagnosis model. In recent years, the dynamic modeling of machine degradation has been extensively studied. Sawalhi and Randall [14,15] constructed a 34 degrees of freedom lumped parameter dynamic model for a gear-bearing system and analyzed the frequency components for different fault types of bearings and gears. Bachar et al. [16] established a realistic nonlinear dynamic model for a spur gear transmission based on the lumped parameter method (LPM) to analyze its vibration response under local tooth face fault. Liu et al. [17] constructed a finite element method (FEM)-based dynamic model for a gearbox and evaluated its confidence by comparing the physical data in the time domain. He et al. [18] established a dynamic model for a planetary gear set based on the rigid–flexible coupling method (RFCM) to investigate its vibration characteristics under normal and fault conditions. Mishra et al. [19] built a rigid–flexible coupling dynamic (RFCD) model for a rolling bearing to

Received October 20, 2022; accepted February 6, 2023

generate its vibration characteristics under different fault conditions and analyzed them using fast Fourier transform (FFT) and envelope spectra analysis. Liu et al. [20] combined the bearing fault mechanism and a dynamic model of planetary gears to generate the corresponding vibration response. They also validated the virtual data based on its frequency features. Song et al. [21] proposed a dynamic model for a marine gearbox based on LPM and FEM and evaluated the generated signal in the frequency domain. El Yousfi et al. [22] constructed an integrated model of a motor-gearbox system that consists of a mathematical model for an induction motor and an LPM-based dynamic model for the gearbox. They evaluated the effectiveness of the simulation signal for the local gear tooth in the frequency domain. Many methods, such as LPM, FEM, and RFCM, have been successfully applied in dynamic modeling to reflect the vibration characteristics of physical parts.

The above studies mainly focus on the vibration mechanism of a gearbox to aid its understanding and provide guidance for fault diagnosis. However, analyses of generated signals are mainly performed in the frequency domain. A small number of studies have focused on updating and optimizing the dynamic model on the basis of the data interaction between virtual and physical entities. Without information about physical–virtual interactions, virtual data reliability cannot be fully validated, which may weaken the effectiveness of the fault diagnosis model when using virtual data to train the model.

Fortunately, as a potential and promising methodology, the digital twin can enhance the data interaction between virtual space and physical entity [23]. The concept of the digital twin was first proposed by Grieves [24] in which a three-dimensional conceptual model, including the physical space, virtual space, and information connection, was presented. Compared with traditional simulation techniques, the digital twin emphasizes the information interaction between physical and virtual spaces. For example, information in the physical space (measured data) can be used to update the virtual model, whereas that in the virtual space (virtual response) can be analyzed to reflect the status of the physical entity, thus guiding the improvement of the operational reliability for the physical entity. With the recent rapid development of emerging technologies, such as sensing, the Internet of Things, and artificial intelligence, the digital twin has attracted increased research attention and has been extensively employed in different fields [25,26]. The digital twin can improve equipment reliability and reduce maintenance cost in the prognostics and health management (PHM) field. The general procedure of the digital twin-driven methodology can be briefly summarized as follows: 1) Establish a high-fidelity virtual model and update it with physical data; 2) utilize the information from the virtual model via signal processing, machine learning, or other techniques to assess the health state of physical assets; 3) provide the maintenance or optimizing operation guidance to the physical entity. The fault diagnoses of machining tools [27], rotor-ball bearing systems [28], air handling units [29], and autoclave equipment [30] have recently been studied, achieving satisfactory performances. For gearboxes, several attempts have been made to monitor gear surface degradation [31], diagnose different fault types [32], and estimate fatigue damage in various components [33]. Using the digital twin, these studies aim to mine valuable knowledge from a virtual model to meet existing challenges in the fault diagnosis field. However, constructing and updating the virtual model are ignored during the process, which may affect the effectiveness and accuracy of these methods. Thus, the construction and updating of a virtual model for fault diagnosis require further investigation.

On the basis of the vibration response analysis, a digital twin-assisted dynamic model updating scheme is proposed to improve the fidelity and reliability of the virtual model. The primary process of the proposed method can be outlined in three steps. First, an initial virtual model is constructed using a dynamic modeling method to mirror the vibration characteristics of the corresponding physical entity, where the operation condition is matched with that of the physical space. Second, the generated data are analyzed via the frequency spectrum to evaluate the feasibility of constructing the model. Finally, a physical–virtual signal interaction method based on a similarity indicator is proposed to dynamically update the virtual model in which parameter sensitivity analysis, surrogate technique, and optimization algorithm are applied to increase efficiency during model updating.

The main contributions of our study can be summarized as follows:

1) A digital twin-assisted dynamic model updating approach toward fault diagnosis is proposed to improve the fidelity of virtual models, where the generated data reliability can be comprehensively evaluated and updated in frequency and time domains.

2) A physical–virtual signal interaction method is proposed to iteratively update a virtual model and minimize the difference between physical and virtual data, which can enhance the generated data quality.

3) The fidelity of the constructed dynamic model is maintained under varying working conditions, which can ensure the performance of the machine fault diagnosis.

The remainder of this paper is organized in the following manner. Preliminary theories regarding the vibration mechanism, polynomial response surface model (PRSM), and optimization algorithm are introduced in Section 2. Details of the proposed model updating are presented in Section 3. An experimental study of a gearbox is presented in Section 4. This paper ends with our conclusions in Section 5.

2 Preliminary

2.1 Gearbox vibration mechanism

In general, the vibration response of a gearbox can be used to assess its health state. Therefore, the vibration response of the generated data can be used to evaluate a virtual model for the machine fault diagnosis.

As described in Ref. [34], the exciting force of a healthy single-stage gearbox contains linear and nonlinear components. Without considering the high-frequency components caused by nonlinear excitation, the frequency components of a healthy gearbox primarily contain the mesh frequency and its harmonics. Thus, excitation force $f(t)$ and vibration response $y(t)$ can be expressed by Eqs. (1) and (2), respectively:

$$f(t)=\sum_{i=1}^{M}a_i\cos(2\pi i f_z t+\theta_i), \tag{1}$$

$$y(t)=h(t)*\left[\sum_{i=1}^{M}a_i\cos(2\pi i f_z t+\theta_i)\right]=\sum_{i=1}^{M}\bar{a}_i\cos(2\pi i f_z t+\bar{\theta}_i), \tag{2}$$

where $*$ represents convolution, a_i and $\bar{a}_i$ are the amplitudes of the exciting force and vibration response, respectively, θ_i and $\bar{\theta}_i$ are the phases of the exciting force and vibration response, respectively, t means time, $h(t)$ represents the transfer function of the gearbox, M is the number of mode order, and f_z is the mesh frequency whose value can be calculated by the following:

$$f_z=z_1 f_{n1}=z_2 f_{n2}, \tag{3}$$

where z_1 and z_2 are the tooth numbers of driving and driven gears, respectively, and f_{n1} and f_{n2} are the rotation frequencies of the input and output gears, respectively.

The amplitude of the corresponding frequency is primarily influenced by the location of the response point, which determines the transfer function.

2.2 Polynomial response surface model

The response surface methodology (RSM) explores the relationship between variables and their corresponding responses [35,36]. PRSM, one of the most popular RSM models, is an explicit, effective, and time-saving model for the surrogating complex dynamic model. PRSM has been widely used in design optimization and structural reliability analyses [37,38]. Its application for model updating can reduce the computational cost of dynamic model optimization. Its fitting accuracy is also highly determined by the setup of sampling points. The Latin hypercube sampling (LHS) method [39] is one of the most popular sampling methods and can generate near-random sample points evenly across all possible values. It is usually adopted to obtain the sampling points during PRSM construction. PRSM can be expressed as follows:

$$\boldsymbol{Y}=\boldsymbol{X}\boldsymbol{\beta}+\boldsymbol{\varepsilon}, \tag{4}$$

where $\boldsymbol{Y}$ is the response vector of sampling points, $\boldsymbol{X}$ is the variable matrix of sampling points, $\boldsymbol{\beta}$ is an unknown coefficient vector, and $\boldsymbol{\varepsilon}$ is the error vector. The least squares method (LSM) is adopted to estimate unknown coefficients by minimizing the error between PRSM and sampling results. Unknown coefficients $\boldsymbol{\beta}$ can be calculated by the following:

$$\boldsymbol{\beta}=\left(\boldsymbol{X}^{\mathrm{T}}\boldsymbol{X}\right)^{-1}\boldsymbol{X}^{\mathrm{T}}\boldsymbol{Y}. \tag{5}$$

The coefficient of determination R^2 is utilized to quantify the fitting accuracy of PRSM, which is calculated as follows:

$$R^2=1-\frac{\sum_{i=1}^{L}(y_i-\tilde{y}_i)^2}{\sum_{i=1}^{L}(y_i-\bar{y})^2}, \tag{6}$$

where y_i is the result of sample point i based on the complex simulation model, $\tilde{y}_i$ is the result of sample point i based on the constructed surrogate model, L is the number of sample points, and $\bar{y}$ is the mean value of the simulation response. An R^2 value closing to 1 indicates that the surrogate model has high fitting precision.

3 Digital twin-assisted virtual model updating method

This section introduces the proposed digital twin-assisted virtual model updating method in detail. Figure 1 shows a flowchart of the proposed method, which is presented in three parts: virtual model construction (Part I), modeling method validation (Part II), and model updating based on the physical–virtual interaction (Part III).

3.1 Part I: virtual model construction

In the first stage, a virtual model is established using a dynamic modeling method (e.g., FEM, LPM, and RFCM) that can mirror the geometric and vibration characteristics (e.g., gear shape, assembly information, and gear dynamics) of the physical entity. To balance computation efficiency and simulation accuracy, RFCM is adopted to construct the dynamic model in this study, which can obtain the virtual response from a particular position (e.g., accelerometer location). In addition, the operating conditions (e.g., the rotary speed of the input shaft and working loading) of the established model should coincide with the settings in the physical entity.

With these steps, an initial virtual model can be built, and the vibration response of the virtual twin can be generated for further analysis.

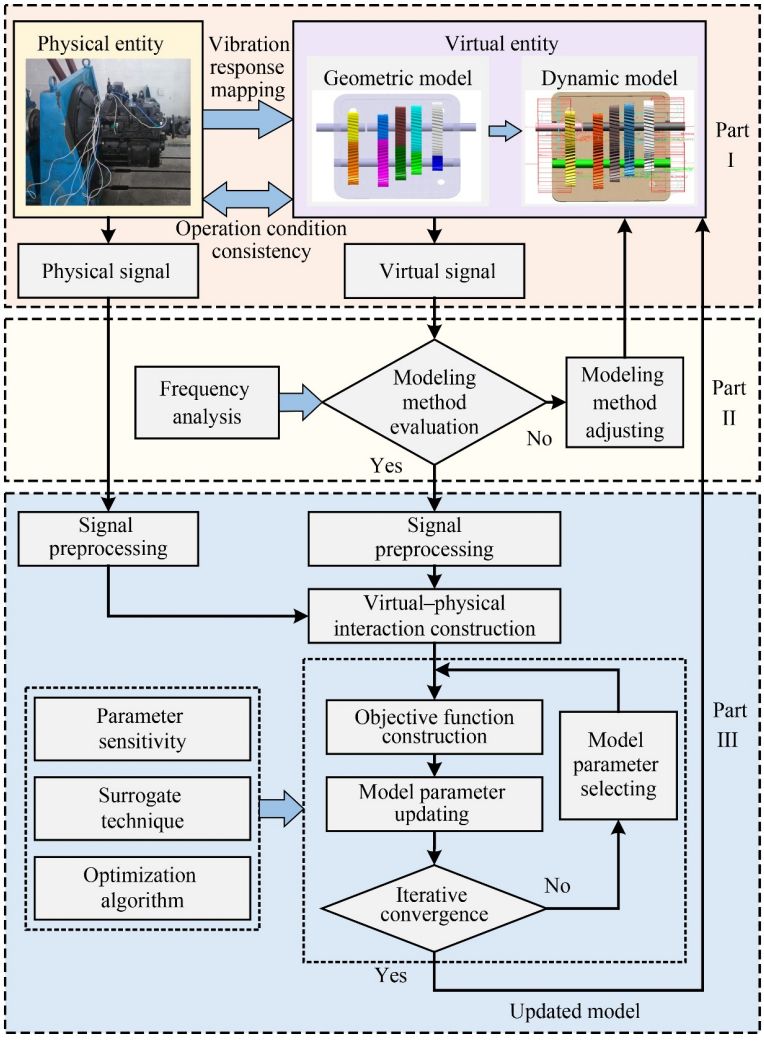

Fig. 1 Flowchart of the digital twin-assisted model updating method.

3.2 Part II: modeling method validation

After the virtual model is constructed, the feasibility of the modeling method should be evaluated, which is fundamental to the efficiency and effectiveness of model updating. According to the operating mechanism of the gearbox, vibration characteristics reflect its healthy state, which can be presented in the frequency domain. Compared with theoretical frequency components, the effectiveness of the modeling method can be evaluated.

In general, the relative error among the main frequency components of the generated and theoretical signals can be selected as the judgment index, which is specified as 5%. If this index meets the requirements, then the modeling method is acceptable for the subsequent stage. Else, the modeling method, such as the gear pair contact and bearing model, should be adjusted. Subsequently, a difference analysis between the generated and experimental signal frequency features should be conducted to determine whether the operating conditions in the dynamic model match those in the physical entity. If this difference cannot satisfy the requirements, then the settings of the working operations in the established model should be updated according to the experimental frequency spectrum.

3.3 Part III: model updating based on the physical–virtual interaction method

To improve the fidelity of the virtual model, a model updating method is proposed based on the physical–virtual interaction, which can be regarded as an optimization process. To minimize the difference between the generated and physical signals, the objective function is defined as follows:

$$\begin{aligned} &\min \|\boldsymbol{R}(\boldsymbol{p})\|_2^2, \quad \boldsymbol{R}(\boldsymbol{p}) = \boldsymbol{X}_{\mathrm{e}} - \boldsymbol{X}_{\mathrm{g}}, \\ &\text{s.t. } \boldsymbol{p}_{\mathrm{L}} \leqslant \boldsymbol{p} \leqslant \boldsymbol{p}_{\mathrm{U}}, \end{aligned} \tag{7}$$

where $\boldsymbol{X}_{\mathrm{e}}$ and $\boldsymbol{X}_{\mathrm{g}}$ represent the physical and generated signals in the time domain, respectively, $\boldsymbol{p} = [p_1, p_2, ..., p_n]$ are the model parameters in the dynamic model, n is the number of these parameters, and $\boldsymbol{p}_{\mathrm{L}}$ and $\boldsymbol{p}_{\mathrm{U}}$ are the lower

and upper bounds of the model parameters, respectively.

To effectively bridge the interaction between physical and virtual spaces, a signal similarity indicator that can be used to evaluate the difference between the generated and physical signals is constructed. In general, the more similar the generated signal is to the physical one, the higher the fidelity of the dynamic model, making the constructed fault diagnosis model based on these data further effective [40,41]. Thus, selecting a suitable signal similarity indicator is significant for monitoring the dynamic model performance during model updating. Cosine similarity, one of the most popular data similarity indicators, has been widely employed in the similarity evaluation of vibration signals for fault diagnosis [17,32]; it can be defined as follows:

$$\boldsymbol{R}(\boldsymbol{p}) = \frac{\boldsymbol{X}_{\mathrm{e}} \cdot \boldsymbol{X}_{\mathrm{g}}}{\|\boldsymbol{X}_{\mathrm{e}}\| \times \left\|\boldsymbol{X}_{\mathrm{g}}\right\|}. \tag{8}$$

To increase efficiency in practical applications, a sensitivity analysis of the signal similarity indicator is conducted as follows:

$$\boldsymbol{S}(\boldsymbol{p}) = \frac{\partial \boldsymbol{R}(\boldsymbol{p})}{\partial p_i}, \quad i \in \boldsymbol{Z}, \ 1 \leqslant i \leqslant n. \tag{9}$$

Sensitive model parameters can be obtained as follows:

$$\boldsymbol{p}_{\mathrm{s}} = [p_{\mathrm{s}1}, p_{\mathrm{s}2}, ..., p_{\mathrm{s}k}], \quad k \in \boldsymbol{Z}, \ 1 \leqslant k \leqslant n, \tag{10}$$

where k is the number of sensitive model parameters.

Then, the surrogate technique (PRSM) is adopted to reduce the computation time of model updating. Correspondingly, the signal similarity indicator can be expressed by a classical third-order PRSM as follows:

$$\begin{aligned}\boldsymbol{R}_{\mathrm{s}}(\boldsymbol{p}_{\mathrm{s}}) = a_0 + \sum_{i=1}^{k} a_i p_{\mathrm{s}i} + \sum_{i=1}^{k} a_{ii} p_{\mathrm{s}i}^2 + \sum_{i>j}^{k} a_{ij} p_{\mathrm{s}i} p_{\mathrm{s}j} \\ + \sum_{i=1}^{k} a_{iii} p_{\mathrm{s}i}^3 + \sum_{i>j}^{k} a_{iij} p_{\mathrm{s}i} p_{\mathrm{s}i} p_{\mathrm{s}j},\end{aligned} \tag{11}$$

where a_* represents the unknown coefficients that are determined by the sampling points and obtained through LSM.

Thus, the objective function can be simplified as follows:

$$\begin{aligned}&\max \boldsymbol{R}_{\mathrm{s}}(\boldsymbol{p}_{\mathrm{s}}), \\ &\text{s.t. } \boldsymbol{p}_{\mathrm{sL}} \leqslant \boldsymbol{p}_{\mathrm{s}} \leqslant \boldsymbol{p}_{\mathrm{sU}},\end{aligned} \tag{12}$$

where $\boldsymbol{p}_{\mathrm{sL}}$ and $\boldsymbol{p}_{\mathrm{sU}}$ are the lower and upper bounds of the sensitive model parameters, respectively.

The firefly algorithm (FA) [42,43] is selected as the optimization algorithm for updating the model. Compared with other algorithms [44,45], FA has the benefits of high optimizing efficiency, reliable accuracy, and easy implementation. The main idea of FA is to simulate the flying and flashing behaviors of fireflies in nature. The movement characteristics of one firefly are related to its brightness. A less bright firefly moves toward a brighter one, and the brightest firefly moves randomly. Every firefly is a potential solution to an optimization problem, and its brightness can be determined by the optimization objective.

Suppose that FA has an initial population of N fireflies in the k-dimensional sensitive model parameter space. The location of the ith firefly is described as $\boldsymbol{p}_{si} = (p_{i1}, p_{i2}, ..., p_{ik})$ (i = 1,2, …,N). If the brightness of firefly j is greater than that of firefly i, then firefly i moves toward firefly j. This movement is expressed as follows:

$$\boldsymbol{p}_{si}^{g+1} = \boldsymbol{p}_{si}^{g} + \beta_0 \mathrm{e}^{-\gamma \cdot r_{ij}^2} \left(\boldsymbol{p}_{sj}^{g} - \boldsymbol{p}_{si}^{g}\right) + \alpha (\mathfrak{I} - 0.5), \tag{13}$$

$$r_{ij} = \left\|\boldsymbol{p}_{si} - \boldsymbol{p}_{sj}\right\| = \sqrt{\sum_{h=1}^{k} (p_{ih} - p_{jh})^2}, \tag{14}$$

where g indicates the gth iteration, β_0 is the attractiveness factor, with a value between 0 and 1, γ is the brightness absorption coefficient, with a common value of 1, r_{ij} represents the distance between fireflies i and j, α is a random parameter that controls movement randomization, with a value between 0 and 1, and $\mathfrak{I}$ is a random vector (k-dimensional) whose values can be selected from a standard Gaussian distribution N(0,1).

3.4 Proposed method procedure

Figure 1 outlines the main procedure of the proposed method, which can be briefly summarized as follows:

Step 1: Build a virtual model (including geometric and dynamic models) and generate virtual signals.

Step 2: Analyze the generated signal using frequency analysis and evaluate the modeling method using the relative error; if the relative error is larger than 5%, then adjust the modeling method.

Step 3: Preprocess the physical and generated signals in the time domain using a filtering algorithm and normalization.

Step 4: Bridge the interaction between physical and generated signals.

Step 5: Determine the optimization model parameters using sensitivity analysis.

Step 6: Establish PRSM to substitute the virtual model and analyze its fitting accuracy.

Step 7: Build the optimization model to update model parameters using FA, and then update the dynamic model.

4 Case study

To validate the proposed model updating method, a case study on a gearbox was carried out.

The structure of a single-stage gearbox is displayed in Fig. 2; it comprises a driving gear, driven gear, input shaft, output shaft, rolling bearings, and gearbox housing.

The geometric parameters and material properties of the gear pair are presented in Table 1. The experiments were performed on a transmission test bench, shown in Fig. 3. Two electric motors were used for driving and loading. Vibration signals were measured using three triaxial accelerometers, which were fixed on the input shaft bearing seat, output shaft bearing seat, and mounting base of the gearbox housing. The sampling frequency was set to 25.6 kHz.

4.1 Model construction

The virtual model should have vibration characteristics similar to those of the physical gearbox. Therefore, a dynamic gearbox model was constructed in virtual space to depict physical properties.

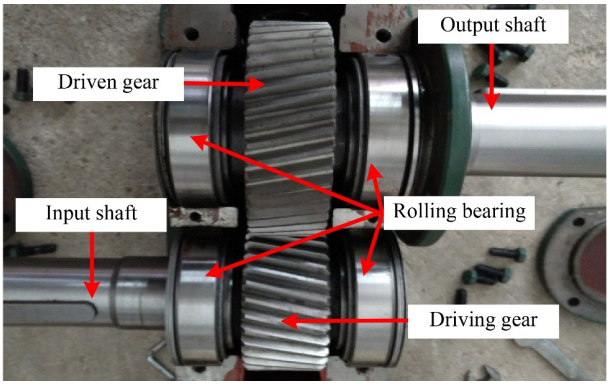

Fig. 2 Structure of a single-stage gearbox.

Table 1 Geometric and material gear parameters

Parameter	Value
Tooth number of driving/driven gears	32/44
Helix angle of driving/driven gears	13°/−13°
Tooth width	35 mm
Normal module	3.5 mm
Normal pressure angle	20°
Density	7800 kg/m^3
Elastic modulus	210 GPa
Poisson's ratio	0.29

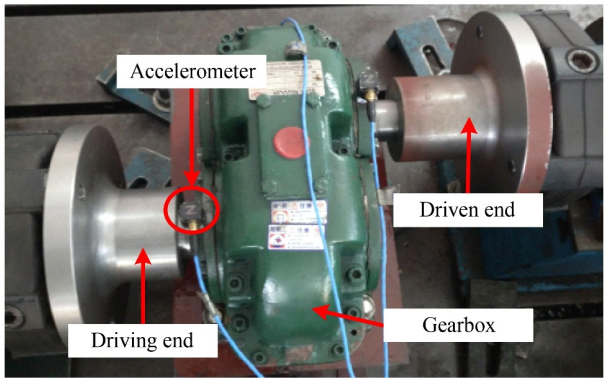

Fig. 3 Experimental test rig for the gearbox.

First, the geometric gearbox model, which is fundamental for dynamic modeling, was built using the commercial software CATIA. Specifically, the geometric models of the gear pair and shafts were established according to their specific parameters, and the gearbox housing was simplified by ignoring a few detailed structures (e.g., stiffeners) to improve modeling efficiency.

Second, an RFCD model for the gearbox was constructed using the commercial software MSC ADAMS. Components such as gear pairs and shafts were assumed to be the Rigid Body whose characteristics were determined by their geometric structures and materials. Instead, the gearbox housing was considered to be the Flexible Body, which was processed with finite elements using the HyperMesh–OpiStruct software. Moreover, fixed joints were used to fasten gears to their corresponding shafts and fix the gearbox housing to the ground. The rotational joint motion of the input shaft was set to simulate the driving motor, whereas the torque applied force of the output shaft was set to add the working load. To reduce analysis costs, rolling bearings were simplified as the bushing force to build a vibration transfer bridge between the shafts and gearbox housing.

Finally, the contact pair between the gear pair, which is the most critical factor in the vibration characteristics of the RFCD model, was simulated by the contact force [19,46]. This model was constructed using tangential and normal contact forces. Specifically, the Coulomb friction model, which is mainly determined by friction coefficients (static C_{sf} and dynamic C_{df}) and transonic speeds (static V_{st} and dynamic V_{dt}), was selected to simulate tangential contact force. Normal contact force was modeled using the impact function, which was formulated with contact stiffness K, damping coefficient C_D, force exponent e_F, and penetration depth D_P. K was calculated according to Hertzian contact theory as follows:

$$K = \frac{4}{3} r_e^{\frac{1}{2}} E_e , \tag{15}$$

$$\frac{1}{r_e} = \frac{1}{r_1} + \frac{1}{r_2} , \tag{16}$$

$$\frac{1}{E_e} = \frac{1-\nu_1^2}{E_1} + \frac{1-\nu_2^2}{E_2} , \tag{17}$$

where r_1 and r_2 represent the equivalent radii, ν_1 and ν_2 are Poisson's ratios of the gears, and E_1 and E_2 represent the elastic moduli of the gears. The values of the equivalent radius are approximately equal to the pitch radius of the gears.

The initial values of K, C_D, e_F, and D_P are listed in

Table 2. The constructed RFCD gearbox model is shown in Fig. 4.

An experiment of the gearbox under one operating condition was conducted, which was called the base operation condition. Specifically, the operating speed of the driving motor was 1000 r/min, and the load torque was 150 N·m. Accordingly, the operation conditions of the RFCD model were identical to those in this experiment in which revolute joints and the torque applied force were set at 6000°/s and 150 N·m, respectively. The analysis step size was set to 1/10000 s.

The experimental signal was measured using an accelerometer attached to the bearing seat of the input shaft. The generated signal was collected using a virtual sensor, as illustrated in Fig. 4. This signal, with a duration of 0.2 s, is shown in Fig. 5; this signal is relatively clean without any noise interference.

4.2 Modeling method analysis

To validate the effectiveness of RFCM, an analysis of the generated response in the frequency domain was conducted. The frequency spectrum of the generated signal was obtained using FFT analysis, as shown in Fig. 6(a). This figure shows three apparent peaks in the frequency spectrum appearing at 533.9, 1067.0, and 1601.0 Hz. According to Eqs. (2) and (3), the main frequency components of the gearbox, in theory, are 533.3, 1066.7, and 1600.0 Hz, with a speed of 1000 r/min. The frequency spectrum of the experimental signal was calculated and is presented in Fig. 6(b); the main frequency components were 533.8, 1068.0, and 1602.0 Hz. From these results, the difference between the main frequency components of the generated response and the theoretical values was below 1%, and the gap between these frequency features between virtual and experimental signals was limited. Owing to the manufacturing and assembly errors of the gearbox, which are difficult to simulate quantitatively, modulation sidebands in the experimental frequency spectrum can be found. In addition, noise from sensors, data acquisition equipment, and other devices was always present in the experiment. Unfortunately, these factors cannot be reliably considered in the RFCD model, which leads to differences in the frequency components of virtual and experimental signals.

In summary, the above results demonstrate that the generated response achieves good effectiveness in the

Table 2 Contact force model details

Parameter	Value
Static friction coefficient C_{sf}	0.1
Static transonic speed V_{st}	1 mm/s
Dynamic friction coefficient C_{df}	0.08
Dynamic transonic speed V_{dt}	10 mm/s
Contact stiffness K	8.6×10^5 N·s/m$^{3/2}$
Force exponent e_F	2.0
Damping coefficient C_D	86 N·s/mm
Penetration depth D_P	0.1 mm

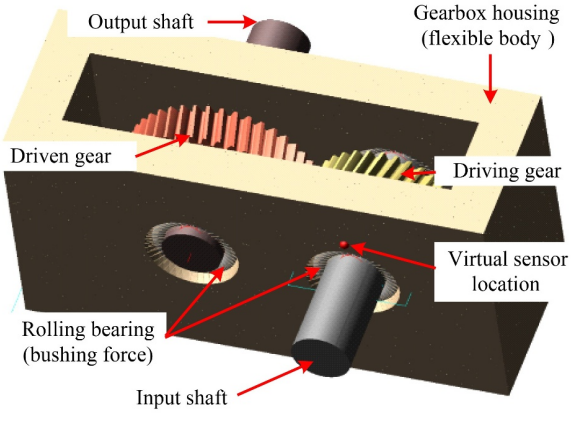

Fig. 4 Rigid–flexible coupling dynamic model of the gearbox analyzed in this study.

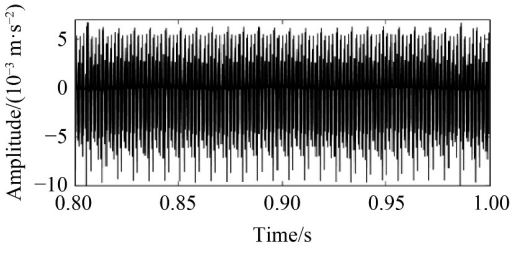

Fig. 5 Generated vibration response.

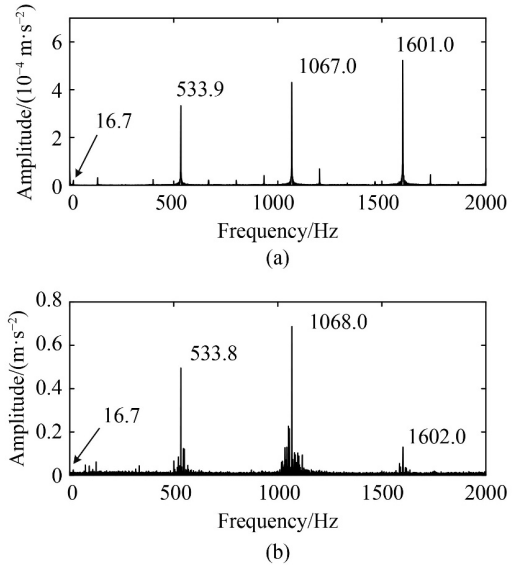

Fig. 6 Frequency spectra of virtual and experimental signals: (a) virtual and (b) experimental frequency spectra.

frequency domain, which implies that the modeling method of the constructed RFCD model is feasible.

4.3 Signal similarity construction

The signal similarity indicator was constructed to establish a bridge for the information interaction between virtual and experimental entities, which can also be used to improve the fidelity of the RFCD model.

Virtual and experimental signals were resampled at 10 kHz to make their time intervals consistent and then normalized to minimize the effect of the vibration transfer path caused by the simplification of the bearing and gearbox housing. Signals were then preprocessed using a digital band-pass filter ([300, 1200] Hz) to reduce noise interference. Subsequently, these signals, with a duration of 0.5 s, were selected, and their cosine similarity was calculated. Using Eq. (8), the cosine similarity value was 0.689, which is greater than 0.6 and indicates a satisfactory consistency [17,32].

Virtual and experimental signals are shown in Fig. 7, demonstrating that the cosine similarity of the signals can be used to evaluate the generated data quality and model fidelity.

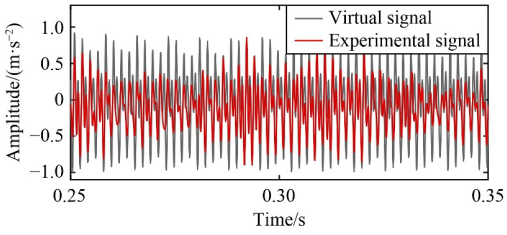

Fig. 7 Comparison between virtual and experimental signals.

4.4 RFCD model updating

Based on the constructed cosine similarity, the information interaction between virtual and experimental gearboxes was established to update the RFCD model. In this model, the material properties of components and contact model between gear pairs may affect vibration characteristics. With this interaction, the fidelity of the RFCD model was improved by optimizing model parameters. To increase optimization efficiency, parameter sensitivity analysis and PRSM were adopted.

4.4.1 Parameter sensitivity analysis

The parameter sensitivity analysis, which is a crucial process to decrease the calculation time of the RFCD model updating, is outlined in this section; it is used to screen crucial factors affecting the cosine similarity between virtual and experimental signals.

In general, many parameters in the RFCD model influence cosine similarity, such as contact stiffness, contact damping coefficient, force exponent, penetration depth, elastic modulus, and density whose analysis scopes are given in Table 3. Figure 8 shows the sensitivity analysis of these parameters concerning cosine similarity. Changes in the elastic modulus, density, and penetration depth of gears have a negligible effect on cosine similarity, whereas the K, C_D, and e_F significantly affect the cosine similarity value. Therefore, these three parameters were selected as optimization parameters to update the RFCD model.

Table 3 Model parameter changes

Parameter	Range
Contact stiffness K	$[4.3 \times 10^5, 12.9 \times 10^5]$ N/mm$^{3/2}$
Damping coefficient C_D	[86, 860] N·s/mm
Force exponent e_F	[1.5, 2.5]
Penetration depth D_P	[0.05, 0.15] mm
Elastic modulus of gears E	[179, 242] GPa
Gear density ρ	[6600, 9000] kg/m^3

4.4.2 PRSM construction

To improve the model updating efficiency and its applicability, a reliable surrogate model must be constructed to replace the RFCD model. Generating 1-s data for the gearbox RFCD model takes approximately five minutes running on a PC with a Core i9-9900 CPU, 32G RAM, and GeForce GTX 1050Ti GPU, which do not meet the requirements of real applications. In recent years, PRSM has been successfully applied to the analysis and optimization of complex systems. The computation time of RFCD model updating can be dramatically reduced using PRSM; the implicit relationship between cosine similarity and model updating parameters can be approximated with few simulation experiments based on the RFCD model.

To obtain a suitable PRSM, the performances of second- and third-order PRSMs were analyzed here. To reduce the impacts of different variable scales, parameters were normalized from 0 to 1 through min–max normalization. During the PRSM construction process, each simulation experiment was expressed as a sampling point, constituted by the updating parameters. Six groups of the training sample set for constructing PRSM, namely, 25, 30, 35, 40, 45, and 50 sample points, were achieved using the LHS method. Meanwhile, one group of the testing set, consisting of 20 sample points for evaluating the performance of the constructed PRSM, was also obtained using the LHS method.

Based on the RFCD model of the gearbox, virtual signals were generated, and cosine similarity was calculated. Thus, six PRSMs were established using the LSM method with corresponding sample sets and cosine

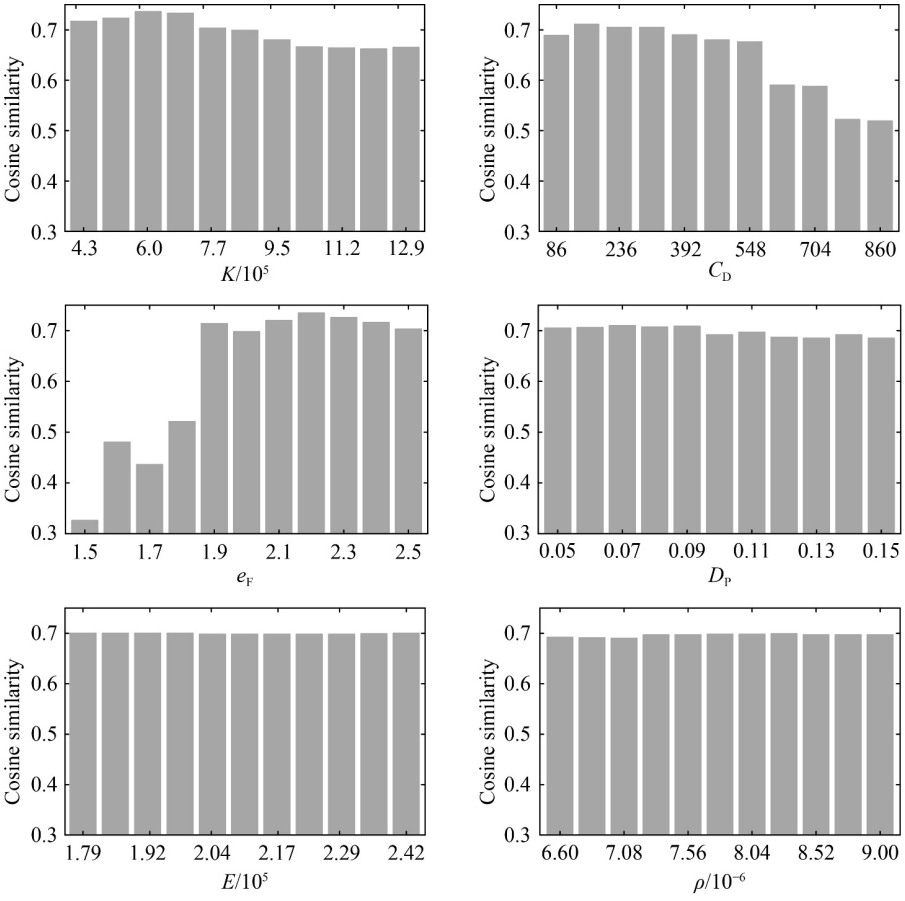

Fig. 8 Sensitivity analysis of parameters on cosine similarity.

similarities. R^2 was utilized to quantify the goodness of fit of each PRSM, and these results are shown in Fig. 9. The R^2 of the third-order PRSM reached 0.97 and remained steady with an increase in sample points, whereas that of the second-order PRSM stabilized at approximately 0.94; thus, the goodness of fit was lower for the second-order PRSM than that for the third-order PRSM. Furthermore, the cosine similarity relative error between these PRSMs and the RFCD model using the testing set was analyzed, and the results are shown in Fig. 10. The performance of the third-order PRSM was slightly better than that of the second-order PRSM when the number of simulation experiments was greater than 40. For example, when the number of simulation experiments was 45, the maximum and mean relative errors were 0.067 and 0.027, respectively. For the third-order PRSM, when the number of simulation experiments was 25, R^2 reached 0.991, and the maximum relative error was 0.45, indicating the overfitting phenomenon. These results illustrate that the fitting precision of the third-order PRSM with 45 sample points can achieve satisfactory results and that this model can be used as a surrogate for the RFCD model. Given the normalized values of contact stiffness (t_1), contact damping coefficient (t_2), and force exponent (t_3), PRSM was established as follows:

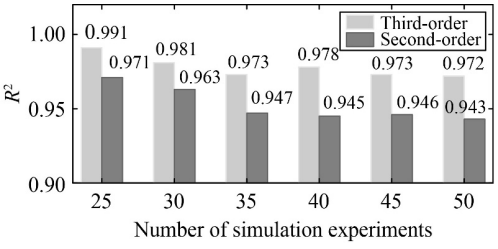

Fig. 9 R^2 for different sample points.

$$\begin{aligned} f(t_1,t_2,t_3) = {} & 0.6349 - 0.8374t_1 - 0.0945t_2 + 0.5874t_3 \\ & + 0.1797t_1^2 + 0.7383t_2^2 - 0.7154t_3^2 + 1.8013t_1t_2 \\ & + 0.2717t_1t_3 - 0.6715t_2t_3 + 0.3009t_1^3 - 0.6105t_2^3 \\ & + 0.0692t_3^3 - 0.6517t_1^2t_2 - 0.4633t_1^2t_3 - 0.8417t_2^2t_1 \\ & + 0.2818t_2^2t_3 + 0.0397t_3^2t_1 + 0.2283t_3^2t_2, \end{aligned} \tag{18}$$

where $f(t_1,t_2,t_3)$ is the cosine similarity between virtual and experimental signals.

4.4.3 Model updating based on FA

The higher the fidelity of the RFCD model, the greater the similarity between the experimental and generated signals. Thus, cosine similarity was selected as the

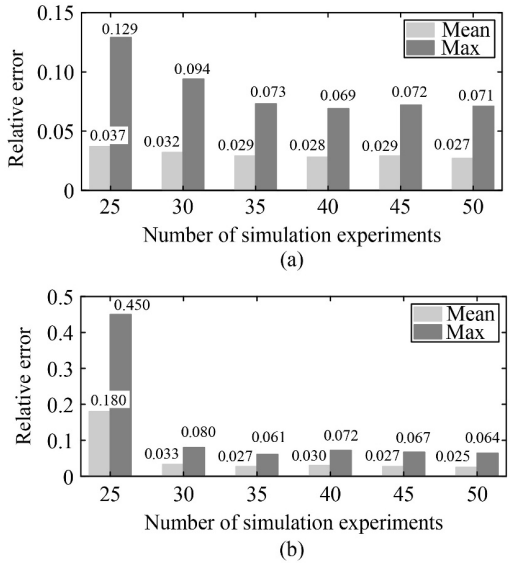

Fig. 10 Relative errors of the (a) second-order and (b) third-order polynomial response surface models using the testing set.

optimization objective. The search space of the optimization parameters can be expressed as follows:

$$\begin{aligned} 4.3\times10^5 \leqslant K \leqslant 12.9\times10^5,\\ 86 \leqslant C_{\mathrm{D}} \leqslant 860,\\ 1.5 \leqslant e_{\mathrm{F}} \leqslant 2.5. \end{aligned} \tag{19}$$

Furthermore, the optimization model with the normalized variable can be expressed as follows:

$$\begin{aligned} &\max f(t_1,t_2,t_3)\\ &\text{s.t. } t_i \in [0,\ 1],\ i=1,2,3, \end{aligned} \tag{20}$$

where t_i represents normalized updating parameters.

FA was applied for model optimization. The population of fireflies and iteration number were set to 30 and 100, respectively. Through FA optimization, cosine similarity increased from 0.689 to 0.752, indicating the effectiveness of this model updating. The model parameters and their corresponding cosine similarities are listed in Table 4. After parameter updating via the proposed physical–virtual interaction method, the RFCD model can further effectively mirror the vibration characteristics of the experimental gearbox, that is, it can provide a more reliable essential virtual model for generating data.

Table 4 Updated model parameters and similarity results

Value type	Contact stiffness K/(N·mm$^{-3/2}$)	Damping coefficient C_{D}/(N·s·mm^{-1})	Force exponent e_{F}	Cosine similarity
Initial value	8.60×10^5	86	2.00	0.689
Updated value	6.44×10^5	303	2.27	0.752

4.5 RFCD model analysis under different operating conditions

The running condition of the gearbox was varied during actual operation. A good RFCD model should be robust and achieve good performance under varying conditions, meaning that the RFCD model can match the experimental gearbox for different conditions. Therefore, the performance of the RFCD model under different conditions was analyzed in detail.

Three experiments were conducted on a transmission test bench under different operating conditions. The loading and operation speeds of these experiments are listed in Table 5, with their corresponding settings in the updated RFCD model. The generated signals were obtained using an updated model under these operating conditions.

Table 5 Gearbox operating conditions

Condition	Experiment		RFCD model	
	Speed/(r·min^{-1})	Load/(N·m)	Revolute joint/((°)·s^{-1})	Torque applied force/(N·m)
Condition 1	1006	50	6035	50
Condition 2	1005	75	6027	75
Condition 3	1003	100	6021	100
Base condition	1000	150	6000	150

The frequency spectrum of these generated signals was obtained via FFT, and the results are shown in Fig. 11. The main frequency components and theoretical meshing

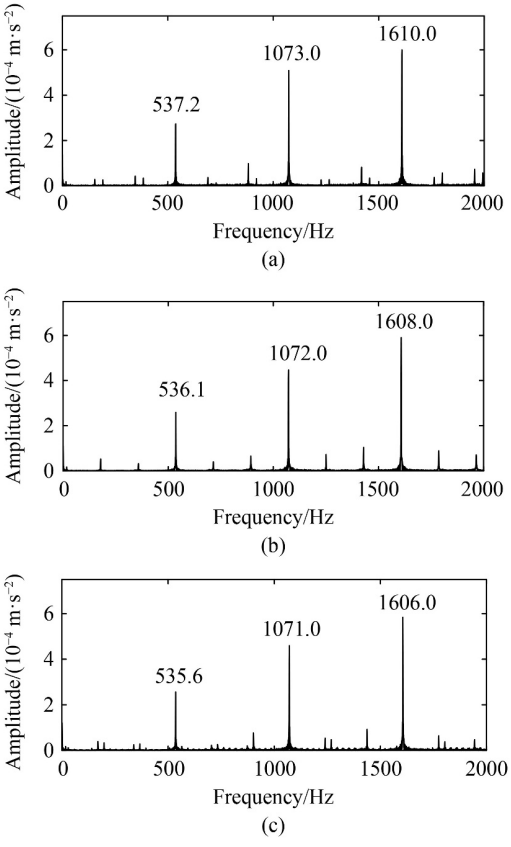

Fig. 11 Frequency spectrum of generated signals under different conditions: (a) Condition 1, (b) Condition 2, and (c) Condition 3.

frequencies for different conditions are listed in Table 6. The relative errors between these main frequency components and the theoretical meshing frequency or its harmonics were less than 1%, suggesting that RFCD model updating is adequate under different operation conditions.

Table 6 Frequency analysis under different conditions

Condition	Meshing frequency or its harmonics/Hz	Virtual main frequency components/Hz
Condition 1	536.5/1073.0/1609.5	537.2/1073.0/1610.0
Condition 2	536.0/1072.0/1608.0	536.1/1072.0/1608.0
Condition 3	534.9/1069.9/1604.8	535.6/ 1071.0/1606.0
Base condition	533.3/1066.7/1600.0	533.9/1067.0/1601.0

The cosine similarity between the experimental and generated signals under different operating conditions was calculated and is shown in Fig. 12. The similarity values under Conditions 1, 2, and 3 were 0.721, 0.744, and 0.762, respectively. Considering these values and that for the base condition together, all values are greater than 0.7, and the fluctuation is limited, which demonstrates that the updated RFCD model remains stable in the time domain. To clearly illustrate the similarity between experimental and generated signals, comparisons are displayed in Fig. 13.

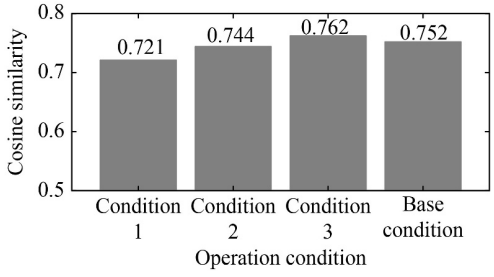

Fig. 12 Cosine similarity under different conditions.

These results verify the effectiveness and stability of the construction of the RFCD model and model updating under different operating conditions, which show strong potential for generating data with high efficiency for fault diagnosis in sample imbalance situations.

5 Conclusions

To obtain an accurate and reliable virtual model of a gearbox, a digital twin-assisted dynamic model updating method was proposed in this study. The main procedure included virtual model construction, modeling evaluation, and physical–virtual-based model updating. Frequency analysis, parameter sensitivity analysis, surrogate technique, and optimization algorithm were employed to improve model updating efficiency. A case study of a gearbox validated the effectiveness of the proposed

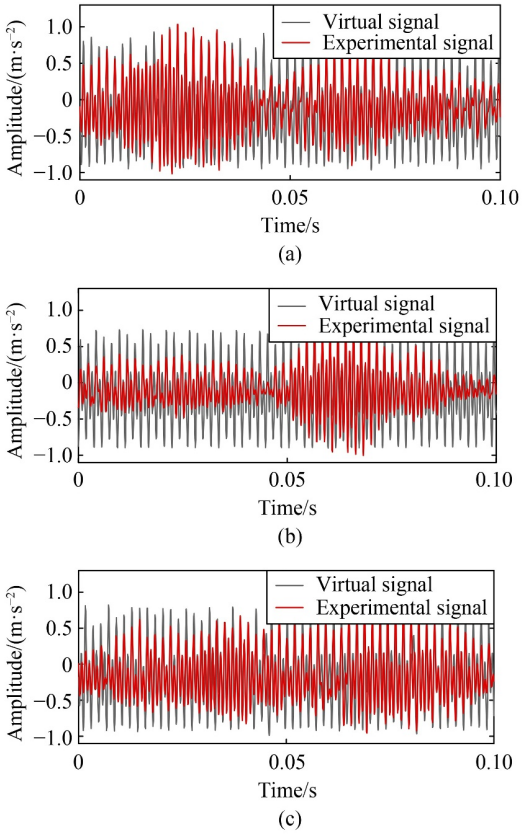

Fig. 13 Comparisons between virtual and experimental signals in the time domain under different conditions: (a) Condition 1, (b) Condition 2, and (c) Condition 3.

method, which convincingly indicates that the proposed method can offer an effective solution for improving the fidelity of the virtual model and enhancing the generated data. In addition, the constructed model with digital twin-assisted updating can achieve good performance under different operating conditions.

In future works, different mechanisms to generate fault data will be investigated. The generated data for different fault types will also be validated according to the corresponding gear failure mechanism; in this way, the data can be effectively supplemented into the training during fault diagnosis model construction. Moreover, advanced signal processing techniques and new-generation machine learning algorithms will be considered to further reduce the gap between physical and virtual entities and improve data-driven fault diagnosis in real-world applications.

Nomenclature

Abbreviations

FA	Firefly algorithm

FEM	Finite element method
FFT	Fast Fourier transform
LHS	Latin hypercube sampling
LPM	Lumped parameter method
LSM	Least squares method
PHM	Prognostics and health management
PRSM	Polynomial response surface model
RFCD	Rigid–flexible coupling dynamic
RFCM	Rigid–flexible coupling method
RSM	Response surface methodology

Variables

a_i	Amplitude of the exciting force
$\bar{a}_i$	Amplitude of the vibration response
C_{df}	Dynamic friction coefficient
C_{D}	Damping coefficient
C_{sf}	Static friction coefficient
D_{P}	Penetration depth
e_{F}	Force exponent
E	Elastic modulus of gears
$f(t)$	Excitation force
$f(t_1,t_2,t_3)$	Cosine similarity between virtual and experimental signals
f_{n1}, f_{n2}	Rotation frequencies of input and output gears, respectively
f_z	Mesh frequency
g	gth iteration
$h(t)$	Transfer function of the gearbox
k	Number of sensitive model parameters
K	Contact stiffness
L	Number of sample points
M	Number of mode order
n	Number of parameters
$\boldsymbol{p}$	Model parameters in the dynamic model
$\boldsymbol{p}_{\mathrm{L}}$	Lower bound of the model parameters
$\boldsymbol{p}_{\mathrm{s}}$	Sensitive model parameters
$\boldsymbol{p}_{\mathrm{sL}}$	Lower bound of the sensitive model parameters
$\boldsymbol{p}_{\mathrm{sU}}$	Upper bound of the sensitive model parameters
$\boldsymbol{p}_{\mathrm{U}}$	Upper bound of the model parameters
r_1, r_2	Equivalent radius
r_{ij}	Distance between fireflies i and j
R^2	Coefficient of determination
$\boldsymbol{R}(\boldsymbol{p})$	Difference between the generated and physical signals
t_1	Normalized contact stiffness
t_2	Normalized contact damping coefficient
t_3	Normalized force exponent
V_{dt}	Dynamic transonic speed
V_{st}	Static transonic speed
$\boldsymbol{X}$	Variable matrix of sampling points
$\boldsymbol{X}_{\mathrm{e}}$	Physical signal in the time domain
$\boldsymbol{X}_{\mathrm{g}}$	Generated signal in the time domain
$\bar{y}$	Mean value of the simulation response
y_i	Result of sample point i based on the complex simulation model
$\tilde{y}_i$	Result of sample point i based on the constructed surrogate model
$y(t)$	Vibration response
$\boldsymbol{Y}$	Response vector of sampling points
z_1	Tooth number of the driving gear
z_2	Tooth number of the driven gear
α	Random parameter that controls movement randomization
$\boldsymbol{\beta}$	Unknown coefficient vector
β_0	Attractiveness factor
$\boldsymbol{\varepsilon}$	Error vector
γ	Brightness absorption coefficient
ν_1, ν_2	Poisson's ratios of the gears
θ_1	Phase of the exciting force
$\bar{\theta}_i$	Phase of the vibration response
ρ	Density of gears
$\mathfrak{J}$	Random vector (k-dimensional)

Acknowledgements This work was supported in part by the National Key R&D Program of China (Grant No. 2018YFB1702400), the National Natural Science Foundation of China (Grant Nos. 52275111, 52205100, and 52205101), and the Guangdong Basic and Applied Basic Research Foundation, China (Grant Nos. 2021A1515110708 and 2023A1515012856).

Conflict of Interest The authors declare that they have no conflict of interest.

References

1. Chen X F, Wang S B, Qiao B J, Chen Q. Basic research on machinery fault diagnostics: past, present, and future trends. Frontiers of Mechanical Engineering, 2018, 13(2): 264–291
2. Singh V, Gangsar P, Porwal R, Atulkar A. Artificial intelligence application in fault diagnostics of rotating industrial machines: a state-of-the-art review. Journal of Intelligent Manufacturing, 2023, 34(3): 931–960
3. Rajabi S, Saman Azari M, Santini S, Flammini F. Fault diagnosis in industrial rotating equipment based on permutation entropy, signal processing and multi-output neuro-fuzzy classifier. Expert Systems with Applications, 2022, 206: 117754
4. Zhang L F, Zhang F B, Qin Z Y, Han Q K, Wang T Y, Chu F L. Piezoelectric energy harvester for rolling bearings with capability of self-powered condition monitoring. Energy, 2022, 238: 121770
5. Maschler B, Weyrich M. Deep transfer learning for industrial automation: a review and discussion of new techniques for data-driven machine learning. IEEE Industrial Electronics Magazine, 2021, 15(2): 65–75

6. Li X, Shao H D, Lu S L, Xiang J W, Cai B P. Highly efficient fault diagnosis of rotating machinery under time-varying speeds using LSISMM and small infrared thermal images. IEEE Transactions on Systems, Man, and Cybernetics: Systems, 2022, 52(12): 7328–7340
7. Cirrincione G, Kumar R R, Mohammadi A, Kia S H, Barbiero P, Ferretti J. Shallow versus deep neural networks in gear fault diagnosis. IEEE Transactions on Energy Conversion, 2020, 35(3): 1338–1347
8. Li W H, Huang R Y, Li J P, Liao Y X, Chen Z Y, He G L, Yan R Q, Gryllias K. A perspective survey on deep transfer learning for fault diagnosis in industrial scenarios: theories, applications and challenges. Mechanical Systems and Signal Processing, 2022, 167: 108487
9. Zhang X, Huang T, Wu B, Hu Y M, Huang S, Zhou Q, Zhang X. Multi-model ensemble deep learning method for intelligent fault diagnosis with high-dimensional samples. Frontiers of Mechanical Engineering, 2021, 16(2): 340–352
10. Li X, Shao H D, Jiang H K, Xiang J W. Modified gaussian convolutional deep belief network and infrared thermal imaging for intelligent fault diagnosis of rotor-bearing system under time-varying speeds. Structural Health Monitoring, 2022, 21(2): 339–353
11. Schwendemann S, Amjad Z, Sikora A. Bearing fault diagnosis with intermediate domain based layered maximum mean discrepancy: a new transfer learning approach. Engineering Applications of Artificial Intelligence, 2021, 105: 104415
12. Lei Y G, Yang B, Jiang X W, Jia F, Li N P, Nandi A K. Applications of machine learning to machine fault diagnosis: a review and roadmap. Mechanical Systems and Signal Processing, 2020, 138: 106587
13. Liao Y X, Huang R Y, Li J P, Chen Z Y, Li W H. Deep semisupervised domain generalization network for rotary machinery fault diagnosis under variable speed. IEEE Transactions on Instrumentation and Measurement, 2020, 69(10): 8064–8075
14. Sawalhi N, Randall R B. Simulating gear and bearing interactions in the presence of faults: Part I. The combined gear bearing dynamic model and the simulation of localised bearing faults. Mechanical Systems and Signal Processing, 2008, 22(8): 1924–1951
15. Sawalhi N, Randall R B. Simulating gear and bearing interactions in the presence of faults: Part II: simulation of the vibrations produced by extended bearing faults. Mechanical Systems and Signal Processing, 2008, 22(8): 1952–1966
16. Bachar L, Dadon I, Klein R, Bortman J. The effects of the operating conditions and tooth fault on gear vibration signature. Mechanical Systems and Signal Processing, 2021, 154: 107508
17. Liu X Y, Huang H Z, Xiang J W. A personalized diagnosis method to detect faults in gears using numerical simulation and extreme learning machine. Knowledge-based Systems, 2020, 195: 105653
18. He G L, Ding K, Wu X M, Yang X Q. Dynamics modeling and vibration modulation signal analysis of wind turbine planetary gearbox with a floating sun gear. Renewable Energy, 2019, 139: 718–729
19. Mishra C, Samantaray A K, Chakraborty G. Ball bearing defect models: a study of simulated and experimental fault signatures. Journal of Sound and Vibration, 2017, 400: 86–112
20. Liu J, Pang R K, Ding S Z, Li X B. Vibration analysis of a planetary gear with the flexible ring and planet bearing fault. Measurement, 2020, 165: 108100
21. Song C S, Zhu C C, Liu H J, Ni G X. Dynamic analysis and experimental study of a marine gearbox with crossed beveloid gears. Mechanism and Machine Theory, 2015, 92: 17–28
22. El Yousfi B, Soualhi A, Medjaher K, Guillet F. Electromechanical modeling of a motor–gearbox system for local gear tooth faults detection. Mechanical Systems and Signal Processing, 2022, 166: 108435
23. Tao F, Qi Q L. Make more digital twins. Nature, 2019, 573(7775): 490–491
24. Grieves M. Digital Twin: Manufacturing Excellence Through Virtual Factory Replication. White Paper, 2014, 1: 1–7
25. Semeraro C, Lezoche M, Panetto H, Dassisti M. Digital twin paradigm: a systematic literature review. Computers in Industry, 2021, 130: 103469
26. Rasheed A, San O, Kvamsdal T. Digital twin: values, challenges, and enablers from a modeling perspective. IEEE Access, 2020, 8: 21980–22012
27. Deebak B D, Al-Turjman F. Digital-twin assisted: fault diagnosis using deep transfer learning for machining tool condition. International Journal of Intelligent Systems, 2022, 37(12): 10289–10316
28. Farhat M H, Chiementin X, Chaari F, Bolaers F, Haddar M. Digital twin-driven machine learning: ball bearings fault severity classification. Measurement Science & Technology, 2021, 32(4): 044006
29. Hosamo H H, Svennevig P R, Svidt K, Han D, Nielsen H K. A digital twin predictive maintenance framework of air handling units based on automatic fault detection and diagnostics. Energy and Building, 2022, 261: 111988
30. Wang Y C, Tao F, Zhang M, Wang L H, Zuo Y. Digital twin enhanced fault prediction for the autoclave with insufficient data. Journal of Manufacturing Systems, 2021, 60: 350–359
31. Feng K, Ji J C, Zhang Y C, Ni Q, Liu Z, Beer M. Digital twin-driven intelligent assessment of gear surface degradation. Mechanical Systems and Signal Processing, 2023, 186: 109896
32. Lou Y X, Kumar A, Xiang J W. Machinery fault diagnosis based on domain adaptation to bridge the gap between simulation and measured signals. IEEE Transactions on Instrumentation and Measurement, 2022, 71: 1–9
33. Moghadam F K, Nejad A R. Online condition monitoring of floating wind turbines drivetrain by means of digital twin. Mechanical Systems and Signal Processing, 2022, 162: 108087
34. Li Y Z, Ding K, He G L, Lin H B. Vibration mechanisms of spur gear pair in healthy and fault states. Mechanical Systems and Signal Processing, 2016, 81: 183–201
35. Khuri A I, Mukhopadhyay S. Response surface methodology. Wiley Interdisciplinary Reviews Computational Statistics, 2010, 2(2): 128–149
36. Ma R B, Dong L H, Wang H D, Chen S Y, Xing Z G. Response surface regression analysis on FeCrBSi particle in-flight properties by plasma spray. Frontiers of Mechanical Engineering, 2016, 11(3): 250–257

37. Bertocci F, Fort A, Vignoli V, Shahin L, Mugnaini M, Berni R. Assessment and optimization for novel gas materials through the evaluation of mixed response surface models. IEEE Transactions on Instrumentation and Measurement, 2015, 64(4): 1084–1092
38. Yi P X, Dong L J, Shi T L. Multi-objective genetic algorithms based structural optimization and experimental investigation of the planet carrier in wind turbine gearbox. Frontiers of Mechanical Engineering, 2014, 9(4): 354–367
39. Sheikholeslami R, Razavi S. Progressive latin hypercube sampling: an efficient approach for robust sampling-based analysis of environmental models. Environmental Modelling & Software, 2017, 93: 109–126
40. Huang R Y, Li J P, Liao Y X, Chen J B, Wang Z, Li W H. Deep adversarial capsule network for compound fault diagnosis of machinery toward multidomain generalization task. IEEE Transactions on Instrumentation and Measurement, 2021, 70: 1–11
41. Cao H R, Shao H D, Zhong X, Deng Q W, Yang X K, Xuan J P. Unsupervised domain-share CNN for machine fault transfer diagnosis from steady speeds to time-varying speeds. Journal of Manufacturing Systems, 2022, 62: 186–198
42. Yang X S. Firefly algorithms for multimodal optimization. In: Watanabe O, Zeugmann T, eds. Stochastic Algorithms: Foundations and Applications. Berlin: Springer, 2009, 169–178
43. Kumar V, Kumar D. A systematic review on firefly algorithm: past, present, and future. Archives of Computational Methods in Engineering, 2021, 28(4): 3269–3291
44. Tian Y, Shi T L, Xia Q. A parametric level set method for the optimization of composite structures with curvilinear fibers. Computer Methods in Applied Mechanics and Engineering, 2022, 388: 114236
45. Mokarram V, Banan M R. A new PSO-based algorithm for multi-objective optimization with continuous and discrete design variables. Structural and Multidisciplinary Optimization, 2018, 57(2): 509–533
46. Wang M F, Ceccarelli M, Carbone G. A feasibility study on the design and walking operation of a biped locomotor via dynamic simulation. Frontiers of Mechanical Engineering, 2016, 11(2): 144–158